Int. J. Electrochem. Sci., 13 **(2018)** 2154 – 2163, doi: 10.20964/2018.02.77

International Journal of ELECTROCHEMICAL SCIENCE
www.electrochemsci.org

A Universal Method to Engineer Porous Carbon-based Electrocatalysts from Cow Dung for Oxygen Reduction

Dongsheng Lu[1,2], *Zining Wang*[1], *Jinyun Liao*[2], *Yi Leng*[2], *Zitian Ding*[2], *Guiqiang Diao*[2], *Hui Wang*[1], *Pengxin Zhou*[1,*], *Hao Li*[2,*]

[1] College of Chemistry and Chemical Engineering, Northwest Normal University, Lanzhou 730070, China
[2] School of Chemistry and Materials Engineering, Huizhou University, Huizhou 516007, China
[*]E-mail: zhoupengxin@163.com (P. Zhou); lihao180@126.com (H. Li).

Received: 1 November 2017 / *Accepted:* 18 December 2017 / *Published:* 28 December 2017

The oxygen reduction reaction (ORR) is a crucial process in fuel cell systems, and techniques that will enable high-efficiency ORR are challenging and elusive. Here, we report N-doped carbon materials prepared by the medium temperature molten salt method that not only exhibit remarkable ORR performance with a high onset potential, half-wave potential and small Tafel slope comparable to those of state-of-the-art Pt/C catalysts, but also possess long-term stability. This work represents a solid step toward high-efficiency oxygen reduction.

Keywords: Oxygen reduction, Fuel cells, Electrocatalysts, N-doped carbon materials, Molten salt method

1. INTRODUCTION

With the over-consumption of petroleum and the resultant environmental problems, it is inevitable that the usage of fossil fuels will greatly decrease, and alternatives will be sought for new types of power sources [1-3]. Fuel cells have demonstrated good safety, high energy, and considerable power densities and may fill the gap between rechargeable batteries and traditional power sources [4]. Over the past few years, many researchers have attempted to develop advanced electrode materials, especially for oxygen reduction reaction (ORR) catalysts, because catalysts are one of the most important factors in working fuel cells [5].

It is well known that Pt has been regarded as the ideal electrocatalyst for the ORR with relatively high current density and low overpotential [6-8]. However, the scarcity of Pt and its high

cost, together with weak stability and low tolerance to methanol, have severely hindered its commercial applications [7-9]. In recent years, vast endeavors have focused on developing low-cost precious metals or metal-free catalysts as alternatives to expensive and scarce Pt, among which carbon integrated with nitrogen represents a group of promising substitutes for Pt-based catalysts because of the low-cost and high ORR activity [10-15]. It has been demonstrated that N-doped carbon materials are very active towards the ORR and may act as substitutes for noble metal catalysts. Thus, it is an urgent challenge to develop a low-cost, highly-efficient, and highly-reproducible method for fabricating N-doped carbon materials for ORR catalysts. [16-21].

NaOH is a strong alkali, which has been used as an etching agent in the preparation of porous carbon, which is utilized to mechanochemically super-polish the surface of carbon materials. However, it is strongly corrosive and can cause damage to equipment. A solvent that is stable at high temperatures is likely to be compatible in this adverse situation. Inspired by this idea, in the current study, NaOH was introduced into the NaCl molten salt medium as a surface-etching agent to prepare mesoporous N-doped carbon with a tunable porous structure. Cow dung (CD), which is a precursor of carbon materials, was selected as the biomass waste that contained C and N sources, and melamine was utilized as an auxiliary component that was carbonized at elevated temperature with NaCl/NaOH[13]. The results show that the existence of NaOH has a large impact on the mesoporous structure and specific surface area. The as-prepared porous N-doped carbons were tested as electrocatalysts for the ORR. The N-doped carbon exhibits comparable ORR activity to that of commercial Pt/C with outstanding durability.

2. EXPERIMENTAL

2.1. Preparation of CD-derived porous N-doped carbons

CD was collected from cattle farms in Lanzhou, China. The reagents used were of analytical grade. In the experiments, the amount of CD was fixed at 1 g, the molar ratio of NaCl/NaOH at 100, and its mass was fixed at 10 g.

The detailed procedure for preparing mesoporous N-doped carbon derived from CD is as follows: CD was first heated to 80 °C in a drying cabinet for 4 days, and then the dried CD was sifted through an 80-mesh sieve to remove the large particles. Then, 1 g of dried CD and 1 g melamine was mixed with 10 g of NaCl/NaOH mixture and ball milled in a zircon jar at 600 rpm for 6 hours. After that, the mixture was loaded into a ceramic crucible and then placed in an inert gas tube furnace. The temperature was raised to 900 °C under a nitrogen atmosphere at a heating rate of 2 °C min^{-1}, and the temperature was maintained for 1 hour. Subsequently, the temperature was cooled to room temperature at a cooling rate of 5 ^{o}C min^{-1}. The obtained product was immersed into 400~500 mL of H_2O and magnetically stirred for 2 h. It was then filtered, and the product was dried for 12 h in a vacuum oven at 90 °C. Afterwards, the carbon material was immersed in 2 M HNO_3 solution for one day to remove inorganic insoluble components. After acid washing, the sample was repeatedly washed with ultrapure water until the pH of the filtered water became neutral, and then it was dried at 90 °C in a vacuum oven again. The final N-doped carbon was labeled as M-CD.

2.2. Physical characterizations

The morphology of the samples was analyzed with scanning electron microscopy (Carl Zeiss Ultra Plus) The specific surface area was measured at a nitrogen adsorption zone with a relative pressure of 0.05 to 0.25. The total pore volume was measured when the relative pressure was 0.99. Furthermore, the density functional theory (DFT) method was used to calculate the pore size distribution. At an excitation laser beam wavelength of 1064 nm, Raman spectroscopy was recorded with a FT-Raman spectroscope (RFS 100, BRU-KER). The intensity of the D and G peaks was gauged by the height from the top point of each band. X-ray photoelectron spectroscopy (XPS) tests were performed on a PHI-5702 spectrometer. Binding energies were calculated by referencing to the C 1s peak at 285.0 eV.

2.3. Electrochemical characterizations

The ORR activities were performed using a CHI 650D (CH Instruments) advanced electrochemical workstation with a glass carbon (GC) electrode 5 mm in diameter as the working electrode, a Pt wire as the counter electrode, and Ag/AgCl (saturated KCl) as the reference electrode. The GC electrode was polished before every test. Each carbon suspension was prepared by dispersing 2 mg activated carbon in 0.4 mL Nafion/ethanol (0.25% Nafion) solution. After 20 minutes of ultrasonic treatment, 10 μL of the prepared ink was applied to the GC electrode, which was then dried at 25°C. The geometric area of the working electrode was approximately 0.196 cm^2, and the mass loading of each carbon material as well as the commercial 20 wt% Pt/C was approximately 0.255 mg cm^{-2}. When the electrochemical test was being performed, it was ensured that the high-purity N_2 or O_2 used was saturated. Cyclic voltammetry (CV) was performed, with scans between -1 V and 0.2 V (*vs.* Ag/AgCl) with 50 mV s^{-1}. For linear sweep voltammetry (LSV), the scan range was from 0.2 V to -0.8 V (*vs.* Ag/AgCl) with 5 mV s^{-1}. The LSV current in oxygen was subtracted form that of nitrogen, resulting in LSV for the ORR. For long-term stability, continuous CV was performed with scans for 1000 cycles. All potentials initially measured versus the Ag/AgCl electrode were converted to a reversible hydrogen electrode (RHE) scale by adding 0.966 V (the potential of the Ag/AgCl reference measured against RHE).

3. RESULTS AND DISCUSSION

Separation of the mixed salt from the final product can result from the improved molecular mixing of two phases due to the compatibility of carbon sources and eutectic salts at high temperature, and further lead to the formation of nanoporous carbon materials [15]. In this study, NaCl/NaOH mixed salts were selected as the molten salt medium to carbonize CD at elevated temperature. It was found that a porous structure formed during carbon source carbonizing with NaCl/NaOH, and solid NaCl also acts as a pore inducer. The Brunauer-Emmett-Teller (BET) surface area of this as-prepared carbonized M-CD was measured to investigate how the amount of NaCl/NaOH affects the final surface area. The amount of NaCl/NaOH significantly impacted the surface area, as it was observed

that when the amount of NaCl/NaOH was 10 g, the obtained BET surface area was the highest among all the carbonized M-CD samples. Therefore, 10 g of NaCl/NaOH was chosen for further investigation of the effect of the etching agent on porous structure and electrochemical performance.

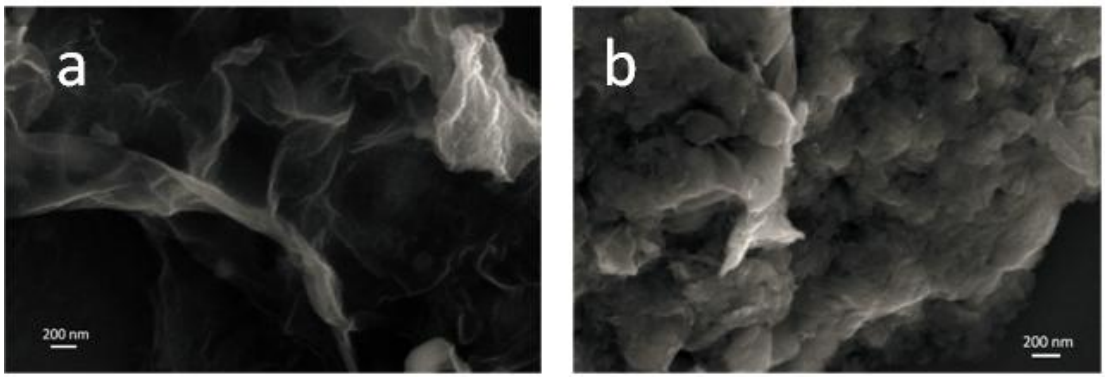

Figure 1. (a) SEM images of M-CD and (b) the carbons prepared without the salt mixture.

SEM images of as-prepared M-CD (a) with and (b) without the salt mixture are presented in Figure 1. As shown in Figure 1a, loose aggregation by thin sheets appears in the SEM images. When M-CD was directly carbonized without any salt, only some irregular-shaped particles with dense structure were obtained (Figure 1b), indicating that the NaCl/NaOH mixture plays an essential role in the formation of sheet-like morphology. It is expected that the loose structure with thin sheets could provide a more accessible active surface for contact with electrolyte that will facilitate mass diffusion between the electrolyte and active materials, and further lead to enhanced electrochemical performance [16].

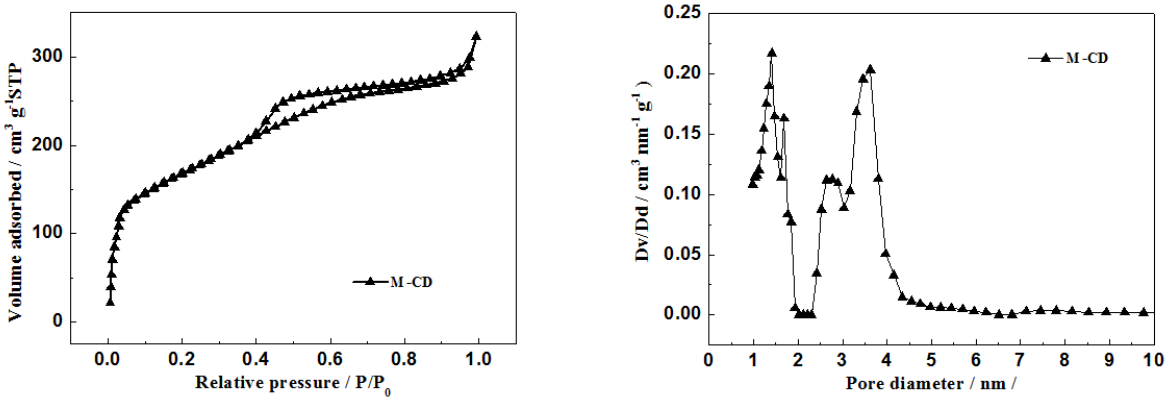

Figure 2. (a) Nitrogen adsorption/desorption isotherms of M-CD and (b) the corresponding pore size distribution curve.

To investigate the effect of NaCl/NaOH on the porous structure, a nitrogen isotherm was adopted to study the porous structures of as-prepared carbon materials (Figure 2). For M-DC, its N_2

isotherm at 77 K exhibits typical type V adsorption/desorption behavior with a small uptake at low relative pressure. The V isotherm originates from the weak gas-solid interaction between micropores and mesoporous solids, which resembles what is obtained for the adsorption of water vapor by microporous materials. This phenomenon indicates that small amounts of micropores and mesopores exist in the carbon materials [18-20]. As shown in Figure 2b, the corresponding pore size distribution curve confirmed this conclusion. The specific surface area of M-CD was calculated via the BET model. The specific surface area of M-CD without the use of the NaCl/NaOH system is 252.8 m^2 g^{-1}, which increased to 598.6 m^2 g^{-1} after NaCl/NaOH was used as the etching agent.

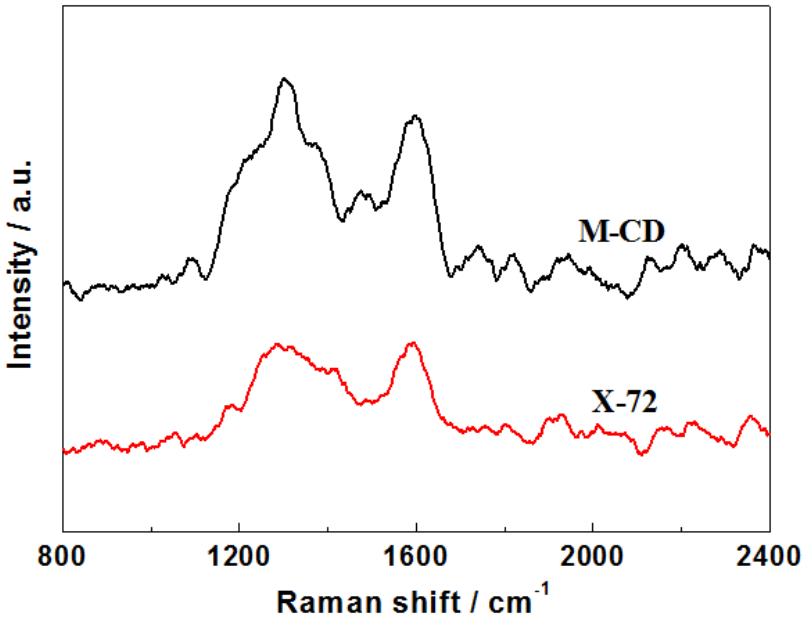

Figure 3. Raman spectra of M-CD and XC-72 carbon.

Figure 3 displays the Raman spectra of M-CD and XC-72 carbon. For both samples, two peaks at approximately 1300 cm^{-1} and 1600 cm^{-1} are observed, which were indexed to the D band and G band, respectively [22, 23]. The Raman D-band results from the atomic displacement and disorder-induced features, which originate from the lattice defect and distortion [13]. In contrast, the G-band results from the in-plane vibration of the E_2 g phonon of sp^2-bonded carbon atoms. The crystallinity of the carbon material can be assessed by the ratio of the relative intensities of the D and G bands [10-13]. For example, a lower ratio of I_D/I_G indicates the high crystallinity of carbon materials [7,13]. The peak intensity ratios of the D-band to G-band (I_D/I_G) for the two samples are 1.24 for M-CD and 1.05 for XC-72 carbon. The I_D/I_G of M-CD is higher in contrast to that of XC-72 carbon, which demonstrates that M-CD possesses a lower graphitic crystalline structure compared with XC-72 carbon. The increase in surface defects of carbon materials can increase the active sites for catalysts, thus enhancing the activity of the catalysts [7,13].

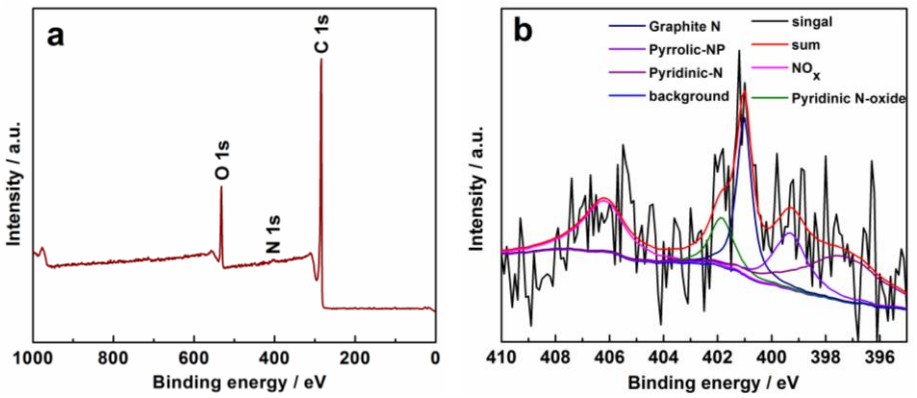

Figure 4. (a) XPS survey spectrum, and (b) N 1s spectrum of M-CD.

XPS measurement was carried out to investigate the sample's surface composition (within a range of 0.1-10 nm) and elemental chemical state. Figure 4a shows the XPS survey spectrum of M-CD with clear signals of C 1s, O 1s, and N 1s, which proves that M-CD is composed of C, O, and N elements. The nitrogen atomic content is approximately 2.2 at. %, and the absence of other elements such as S and Fe suggests that other elements were non-exist or their content was too low for detection. The high -resolution spectra of N1s of M-CD in Figure 4b show five individual nitrogen states, i.e. pyridinic-N at 397.4 eV, pyrrolic-N at 399.4 eV, graphitic-N at 401.0 eV, NO_x at 401.9 eV, and pyridinic N-oxide at 406.2 eV [10-12]. Detailed percentages of these N species in M-CD are estimated by the peak areas. Among these N species, pyridinic-N provides a pair of electrons to bond with the *p*-conjugated rings, and the pyrrolic-N is an excellent electron donor, which can improve the electrochemical performance. Graphitic-N, especially that on the edge, has been proved to bring about lower over-potential for ORR, resulting in improved performance [16, 17]. Analysis indicates that M-CD consists of 31.5% pyridinic-N, 17.1% pyrrolic-N, 21.2% graphitic-N, and 31.2% NOx and pyridinic N-oxide. This indicates that the active N is dominated in M-CD at 401.9 eV, which would give more active sites for catalysis.

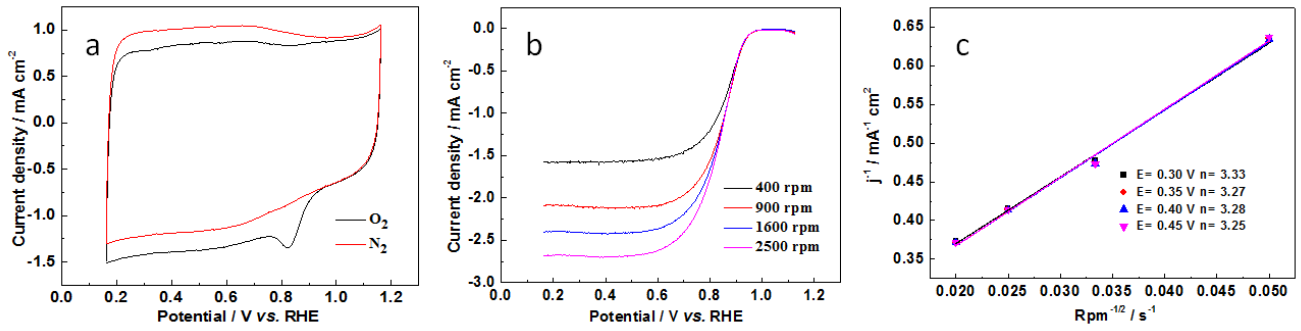

Figure 5. (a) Cyclic voltammograms of M-CD in N_2-saturated and O_2-saturated 0.1 M KOH electrolyte; scan rate: 50 mV s^{-1}; (b) polarization curves for the ORR in O_2-saturated 0.1 M KOH solution on the M-CD electrode at various rotation rates; (c) the Koutecky-Levich (K-L) plots for the ORR derived from (b).

To determine the surface characteristics and ORR activity of M-CD, cyclic voltammograms (CVs) of as-prepared samples were first carried out in nitrogen and oxygen-saturated 0.1 M KOH solutions at a scan rate of 50 mVs^{-1}, as shown in Fig. 5a. The CV curve for M-CD in oxygen-saturated electrolyte shows a reversible and featureless curve with wide voltammetric response, and quasi-rectangular shaped curves were observed, which is a typical behavior of electrochemical capacitors with high specific surface area [23]. In the oxygen-saturated electrolyte, the ORR peak is obvious on M-CD. The electrochemical catalytic ORR on M-CD was investigated in the range of rotating rates from 400 to 2500 rpm, and the results are shown in Figure 5b. All LSVs indicate that increasing the rotating rates will lead to an increase in current density. This observation is understandable because high rotating speeds will reduce the diffusion distance. Figure 4c illustrates the corresponding Koutecky-Levich (K-L) plots for the M-CD that show the inverse current density (j^{-1}) *vs.* the reciprocal of the square root of the rotation speed ($R^{-1/2}$). These K-L plots show good linearity, indicating a first-order dependence of O_2 kinetics on M-CD. The number of transferred electrons for the ORR on M-CD can be computed according to the K-L equation [17, 22, 24]. As displayed in Figure 5c, the number of transferred electrons per O_2 molecule (n) was approximately 3.3, suggesting that the ORR on the M-CD electrode was mainly carried out in a four-electron reaction pathway.

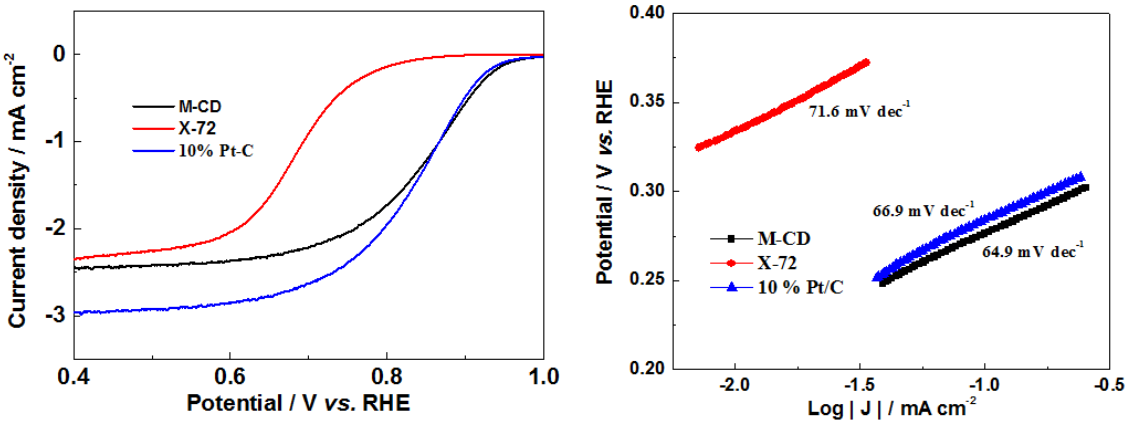

Figure 6. (a) Linear sweep voltammograms of M-CD, commercial carbon, and Pt/C for the ORR in 0.1 M KOH aqueous solution at a scan rate of 5 mV s^{-1} and rotation rate of 1600 rpm; (b) corrected mass transfer Tafel polarization curves of the samples derived from (a).

Figure 6 shows the ORR activity of M-CD, XC-72, and commercial Pt/C (10 wt%) evaluated on a rotating disk electrode (RDE) by linear sweep voltammograms (LSV) in 0.1 mol L^{-1} KOH solution saturated with O_2. As can be observed in Figure 6, the limiting diffusion current, half-wave potential, and onset potential for M-CD is obviously better than those of XC-72. The ORR polarization curves of M-CD and commercial Pt/C exhibit a sharp increase and fleetly reached saturation, indicating that the ORR on both samples was a diffusion-controlled process that was related to the effective $4e^-$ dominated pathway [25-28]. Although the limiting diffusion current of M-CD was less than that of Pt/C, the half-wave potential of M-CD is only 0.01 V higher than that of commercial Pt/C.

The onset potential of M-CD was similar to that of Pt/C, suggesting that there was comparable ORR activity of M-CD to commercial Pt/C. When compared to the most advanced Pt/C catalyst, the Tafel slope of M-CD is very small [6]. These observations demonstrate that M-CD possesses good electrocatalytic ORR properties.

Table 1. A benchmark of our M-CD with previously published values obtained for other biomass-derived carbon samples; all were subject to alkalinity in KOH 0.1 mol L^{-1}.

Catalyst	The literature	The onset potential / V vs. RHE
M-CD	--	0.98
CS2-Fe	10	0.99
Co-CEW	11	0.88
CDB-Fe	12	0.97
CD-Si/Fe	13	0.94
LPCNs	18	0.97
$FeO_{1.4}$/N-C	26	1.0
3D-NCN	27	0.95
N-HPC	28	0.91
CFB	29	0.97

For comparison, the performances of other previously reported carbon catalysts derived from biomass electrodes are listed in Table 1. It can be seen that the catalysts based on M-CD exhibit better catalysis performances in terms of the onset potential of the ORR than other biomass-derived carbon catalysts [11, 13, 27, 28], implying that the M-CD is a promising and effective electrode material for the ORR. Additionally, the catalytic activity of M-CD is comparable to that of some biomass-derived carbon catalysts [12, 29]. It is noteworthy that some of the reported carbon catalysts [10, 26] display an improved catalytic activity compared to the present M-CD electrode, which is possibly attributed to the improved catalytic active sites due to the treatment with Fe salts. This suggests that there is still some room for further improvement in the performances of the present M-CD that can be attained using subsequent processing such as treatment with Fe salts or NH_3 airflow.

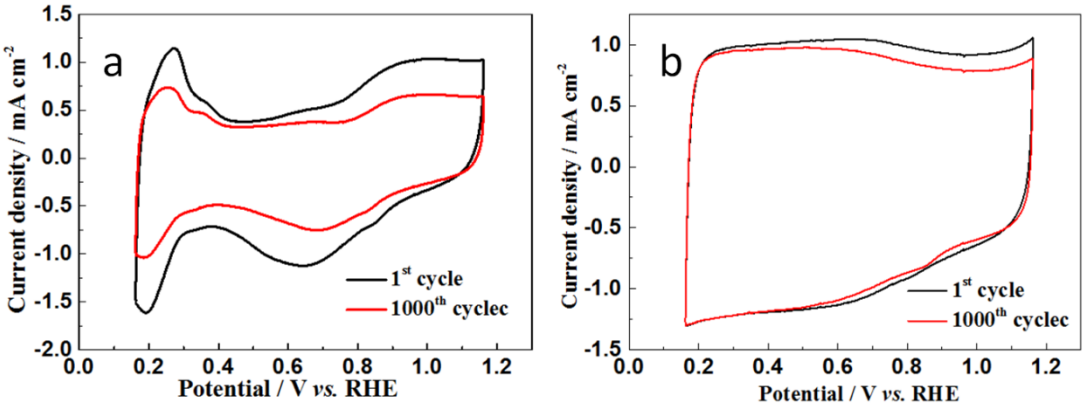

Figure 7. CVs on (a) Pt/C and (b) M-CD before (black curve) and after (red curve) continuous potentiodynamic sweeps for approximately 1000 cycles in N_2-saturated 0.1 M KOH solution at a scan rate of 50 mV s^{-1} at room temperature.

The durability of a catalyst is one of the most crucial factors in current fuel cell technology, and we further compared the electrocatalytic performance of the Pt/C and M-CD catalysts by continuous potentiodynamic sweeps for approximately 1000 cycles in N_2-saturated 0.1 M KOH solution. The CV results are shown in Figure 7. Obviously, the current density of the M-CD remained almost unchanged. In contrast, the Pt/C showed an obvious decrease after 1000 cycles, indicating that the stability of the M-CD is much higher than that of noble catalysts [29, 30].

4. CONCLUSIONS

Porous N-doped carbon from CD was successfully prepared in a molten salt medium with NaOH. The obtained product exhibited sheet-like morphology with a high surface area of 598.6 m^2 g^{-1}. The LSV results shows that the half-wave potential of M-CD is 10 mV more positive than that of commercial Pt/C, indicating that M-CD is more active for the ORR than commercial Pt/C in an alkaline electrolyte. M-CD also possesses long-term operating stability, which potentially makes M-CD a commercially viable cathode catalyst for fuel cells.

ACKNOWLEDGEMENTS
This work was financially supported by the Natural Science Foundation of Guangdong Province (No. 2016A030313120), the High-Level Talent Project of the University in Guangdong Province (No. 184), the Excellent Youth Foundation of the University in Guangdong Province (No.YQ2015154), and the Natural Science Foundation of Huizhou University (No. 20160226013501332).

References

1. N. Kakati, J. Maiti, S. H. Lee, S. H. Jee, B. Viswanathan and Y.S. Yoon, *Chem. Rev.*, 114 (2014) 12397.
2. Q. B. Liu, J. Yang, R. F. Wang, H. Wang and S. Ji, *RSC Adv.*, 7 (2017) 33635.
3. Q. B. Liu, S. Ji, J. Yang, H. Wang, B. G. Pollet and R. F. Wang, *Materials*, 10 (2017) 988.
4. B. E. Logan and K. Rabaey, *Science*, 337 (2012) 686.

5. Z. Y. Mo, R. P. Zheng, H. L. Peng, H. G. Liang and S. J. Liao, *J. Power Sources*, 245 (2014) 801.
6. W. Wang, R. F. Wang, S. Ji, H. Q. Feng, H. Wang and Z. Q. Lei, *J. Power Sources*, 195 (2010) 3498.
7. J. Ding, S. Ji, H. Wang, J. Key, D.J.L. Brett and R.F. Wang, *J. Power Sources*, 374 (2018) 48.
8. J. Ding, S. Ji, H. Wang, B.G. Pollet and R.F. Wang, *Electrochim. Acta*, 255 (2017) 55.
9. G. Zhao, T.S. Zhao, J. Xu, Z. Lin and X. Yan, Int. J. Hydrogen Energy, 42 (2017) 3325.
10. R. F. Wang, K. Wang, Z. H. Wang, H. H. Song, H. Wang and S Ji, *J. Power Sources*, 297 (2015) 295.
11. H. Wang, Z. Zhang, Y. X. Yang, K. Wang, S. Ji, J. Key, Y. Y. Ma and R. F. Wang, *J. Solid State Electrochem.*,19 (2015) 1727.
12. H. Yang, H. S. Li, H. Wang and R. F. Wang, *Fuel Cells*, 15 (2015) 214.
13. Z. Zhang, H. Li, Y. X. Yang, J. Key, S. Ji, Y. Y. Ma, H. Wang and R. F. Wang, *RSC Adv.*, 5 (2015) 27112.
14. A. Dumitru, M. Mamlouk and K. Scott, *Electrochim. Acta*, 135 (2014) 428
15. C. Zhu, H. Li, S. Fu, D. Du and Y. Lin, *Chem. Soc. Rev.*, 45 (2016) 517.
16. J. Xu, L. Shi, C. Liang, H. Wu, J. Lei, D. Liu, D. Qu, Z. Xie, J. Li and H. Tang, ChemElectrocChem., 4 (2017) 1148.
17. Z. B. Yang, J. Ren, Z. T. Zhang, X. L. Chen, G. Z. Guan, L. B. Qiu, Y. Zhang, H. S. Peng, *Chem Rev.*, 115 (2015) 5159.
18. T. B. Zhou, H. Wang, S. Ji, V. Linkov and R. F. Wang, *J. Power Sources*, 248 (2014) 427.
19. R. F. Wang, T. B. Zhou, H. Wang, H. Q. Feng and S. Ji, *J. Power Sources*, 269 (2014) 54.
20. X. P. Wang, S. H. Huo, R. F. Wang, H. Wang, D. Brett and S. Ji, *J. Colloid Interf. Sci.*, 503 (2017) 76.
21. M. Zhou, H.-L. Wang, S. J. Guo, *Chem. Soc. Rev.*, 45 (2016) 1273.
22. H. Wu, L. Shi, J. Lei, D. Liu, D. Qu, Z. Xie, X. Du, P. Yang, X. Hu, J. Li and H. Tang, J. Power Sources, 323 (2016) 90.
23. T. Zhou, H. Wang, S. Ji, H. Feng, R. F. Wang, *Fuel Cells*, 14 (2014) 296.
24. Y. Y. Ma, R. F. Wang, H. Wang, J. Key and S. Ji, *J. Power Sources*, 280 (2015) 526.
25. R. F. Wang, S. J. Liao, H. Y. Liu and H. Meng, *J. Power Sources*, 171 (2007) 471.
26. Y. Ma, H. Wang, J. Key, V. Linkov, S. Ji, X. Mao, Q. Wang and R. Wang, *Int. J. Hydrogen Energy*, 39 (2014) 14777.
27. Y. Chen, H. Wang, S. Ji, W. Lv and R. F. Wang, *Material*, 10 (2017) 1366.
28. X. Ma, S. Feng, and S. Ji, *Int. J. Electrochem. Soc.*, 12 (2017) 7869.
29. H. Wang, K. Wang, H. Song, H. Li, S. Ji, Z. Wang, S. Li and R. Wang *RSC Adv.*, 5 (2015) 48965.
30. K. Wang, H. Wang, S. Ji, H. Feng, V. Linkov and R.F. Wang, *RSC Adv.*, 3 (2013) 12039.